Int. J. Electrochem. Sci., 15 **(2020)** 2157 – 2165, doi: 10.20964/2020.03.21

International Journal of
ELECTROCHEMICAL
SCIENCE
www.electrochemsci.org

One-Step Synthesis of Highly Uniform Fe_3O_4@C Nanospheres as Anode Materials for LIBs

Hui Lv[*], *Yaqin Xue, Xiaohui Feng, Hongxia Wang, Mei Zheng, Baoying Zhang*

College of Food Science and Pharmaceutical Engineering, Zaozhuang University, Zaozhuang 277160, China
[*]E-mail: huiluzz@163.com

Received: 9 November 2019 / *Accepted:* 20 December 2019 / *Published:* 10 February 2020

In this work, highly uniform Fe_3O_4@C nanospheres were synthesized by a one-step solvothermal method with the assistance of a surfactant. The microstructure, morphology, and chemical composition of the obtained samples were characterized by X-ray diffraction, transmission electron microscopy, scanning electron microscopy, and energy dispersion spectrum. The results suggested that the as-prepared highly uniform Fe_3O_4@C nanospheres had an average size of 300 nm in diameter, and a uniform carbon layer with a thickness of about 40 nm was formed on the surface of the Fe_3O_4 nanostructures. The electrochemical performances of prepared Fe_3O_4@C nanospheres electrodes were investigated by cyclic voltammetry, galvanostatic discharge/charge measurements, and electrochemical impedance spectroscopy. Under a current density of 100 mA g^{-1}, the Fe_3O_4@C nanospheres exhibited a high reversible capacity of 539 mAh g^{-1} after 100 cycles, which is 129% retention of the initial charge capacity, and an coulombic efficiency of close to 100%. The prepared Fe_3O_4@C nanospheres (simple strategy, low cost, and good electrochemical properties) can be a practical promising anode material for LIBs.

Keywords: Fe_3O_4@C nanospheres; Highly uniform; Anode material; Lithium-ion battery, Nanocomposites

1. INTRODUCTION

Among the transition metal oxides, magnetite is believed to be one of the most promising electrode materials for LIBs because of its low cost, environmental safety, natural abundance and high theoretical capacity (926 mAh g^{-1})[1,2]. However, Fe_3O_4 suffers from huge volume expansion during charging/discharging, electrical contact loss, and an unstable solid electrolyte interphase (SEI), which limit its practical application in LIBs.

In order to overcome these issues, three well-accepted strategies were put to use. First, the nanoscale Fe_3O_4 particles with variant shapes, such as hollow spheres[3], nanowires[4,5],

octahedrons[6], nanoflakes[7], and hollow nanoellipsoids[8] were developed. Second, the transition metal oxides were combined with other stable metal oxides to enhance their conductivity, including α-Fe_2O_3@Fe_3O_4 heterostructures[9], SnO_2@Fe_2O_3 sandwich cubes[10], tubular MnO_2@Fe_3O_4@C[11], and heterostructured Fe_2O_3/Mn_2O_3[12]. Third, nano carbon materials were introduced into iron oxides to construct Fe_3O_4/carbon composites, such as Fe_3O_4/graphene[13,14], Fe_3O_4/carbon nanotubes [15], Fe_3O_4/carbon coating [16,17], and Fe_3O_4/C fibers[18]. These strategies are considered to buffer the volume change of nanomaterials during charging/discharging and enhance the structural stability at the same time, as well as improving the electrical conductivity of the nanoparticles.

In this study, we reported a facile solvothermal method to fabricate highly uniform Fe_3O_4@C nanospheres. The strategy could directly enhance the electrical conductivity of materials and the carbon coating prevent the Fe_3O_4 spheres from collapsing over long cycles. The highly uniform Fe_3O_4@C nanospheres were found to exhibit a high reversible capacity and excellent cycle performance as anode material for LIBs. Under a current density of 100 mA g^{-1}, the highly uniform structure provides a stable capacity retention of 539 mAh g^{-1} after 100 cycles for lithium ion storage. In addition, the coulombic efficiency is close to 100%.

2. EXPERIMENTAL

Ferrocene (0.6 g) and Tween-80 (0.6 g) were dispersed in 30 mL of acetone with constant magnetic stirring for 20 min, followed by the addition of H_2O_2 (2 mL, 40 wt%). Then the mixture was stirred at room temperature for 2 h. After that, it was transferred to a Teflon-line autoclave with a capacity of 50 mL, and the reaction was maintained at 220 ^oC for 24 h, After cooling to room temperature, the products were separated by a magnet and washed with ethanol and water several times. Finally, the products were dried under a vacuum at 50 ^oC overnight.

The crystallographic and phase structure of materials were identified by X-ray diffraction (XRD, Bruker AXS D8 Advance, Cu*K*α). The morphologies and microstructure of samples were characterized by a Hitachi-S4800 field emission scanning electron microscope (FE-SEM, Hitachi Limited) equipped with an energy dispersion spectrum (EDS) and a transmission electron microscope (TEM, JEOL-JEM2100F) with an electron kinetic energy of 200 kV.

The working electrodes were prepared by mixing acetylene black, active materials (the prepared Fe_3O_4@C nanospheres), and a binder (polyvinylidene fluoride, Kynar FLEX 910, Elf Atochem, Issaquah, WA, USA) with a mass ratio of 15:70:15 in N-methyl pyrrolidone (Fluka Inc., St. Louis, MO, USA) and cast onto a Cu foil current collector. After the working electrodes were dried in a vacuum oven at 80 ^oC overnight, the CR2032 coin cells were assembled in an argon-filled glove box. Li foils were used as the negative electrode, and a Celgard 2300 polypropylene membrane was used as the separator. The electrolyte consisted of 1 M $LiPF_6$ in ethylene carbonate (EC)/ethylmethyl carbonate (EMC)/dimethyl carbonate (DMC) with a weight ratio of 1:1:1 (Guotaihuarong, Zhangjiagang, China). The cycle life and rate capability of the cells were recorded by a battery analyzer (Voir, Huizhou, China) over a range of 0.01-3.00 V (vs. Li+/Li). Cyclic voltammogram (CV) measurements were performed on a CHI660E electrochemical workstation (Chenhua, China) at a scan

rate of 0.1 mV s^{-1} between 0.01 and 3.00 V. Electrochemical impedance spectroscopy (EIS) was carried out on a electrochemical workstation (Solartron 1287, Solartron Co., Britain) in the frequency range from 100 KHz to 0.01 Hz with a perturbation amplitude of 5 mV.

3. RESULTS AND DISCUSSION

The XRD pattern of the as-prepared material is shown in Fig. 1. The lower standard XRD pattern confirmed that all XRD diffraction peaks well corresponded to the pure cubic inverse spinel structure of Fe_3O_4 [space group: Fd3m (227)]. Also, the characteristic peaks of the sample at 2θ = 18.27°, 30.01°, 35.42°, 37.05°, 43.05°, 53.39°, 56.94°, and 62.52° were assigned to the diffraction planes (111), (220), (311), (222), (400), (422), (511) and (440), which is consistent with the standard data (JCPDS no.19-0629). The narrow and sharp diffraction peaks suggest the good crystalline nature of Fe_3O_4 without impurities, while no obvious diffraction peaks related to carbon were observed in the XRD pattern because of the amorphous structure of the carbon layer.

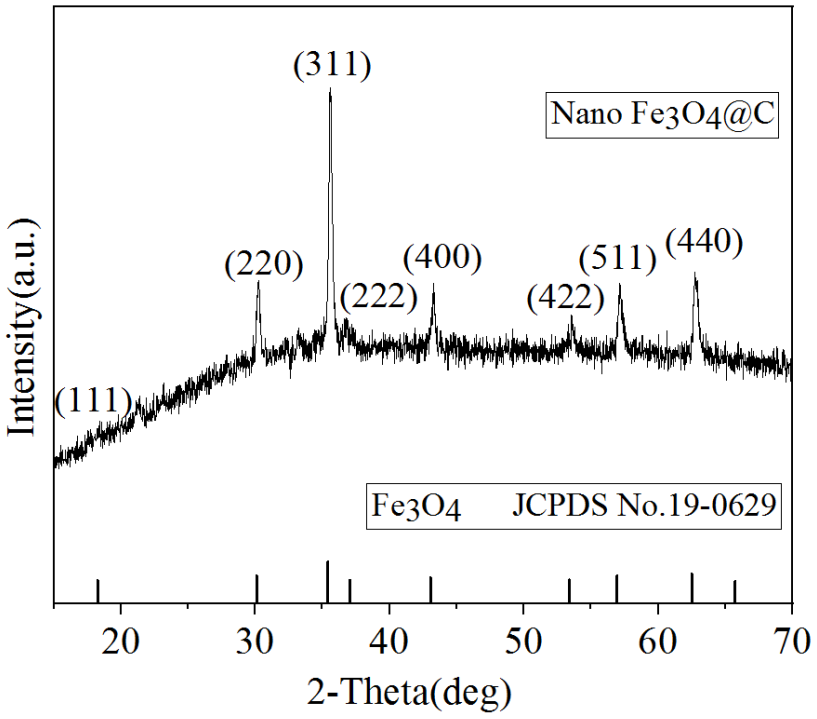

Figure 1. XRD pattern of nano Fe_3O_4@C.

The morphology and structure of Fe_3O_4@C nanospheres were examined by SEM and TEM as shown in Fig. 2. As can be seen, the sphere shaped Fe_3O_4@C nanoparticles with a diameter of 300 nm were observed (Fig. 2(a, b, and c)). The Fe_3O_4@C nanospheres exhibited a well-dispersed and the uniform size. The structure of Fe_3O_4@C was further characterized by TEM (Fig. 2(e, f, and g)). The typical TEM image in Fig. 2f clearly shows that the Fe_3O_4 nanoparticles were uniformly and

effectively coated by an amorphous carbon shell (about 40 nm in thickness). Better cycle stability and rate performance can be achieved by optimizing the morphology and size of the materials or embedding the materials in carbon[19]. Nanospheres provide more space for the Li^+ insertion and extraction reaction and a shorter pathway for Li^+ transfer because of their high specific surface and surface activity[20].

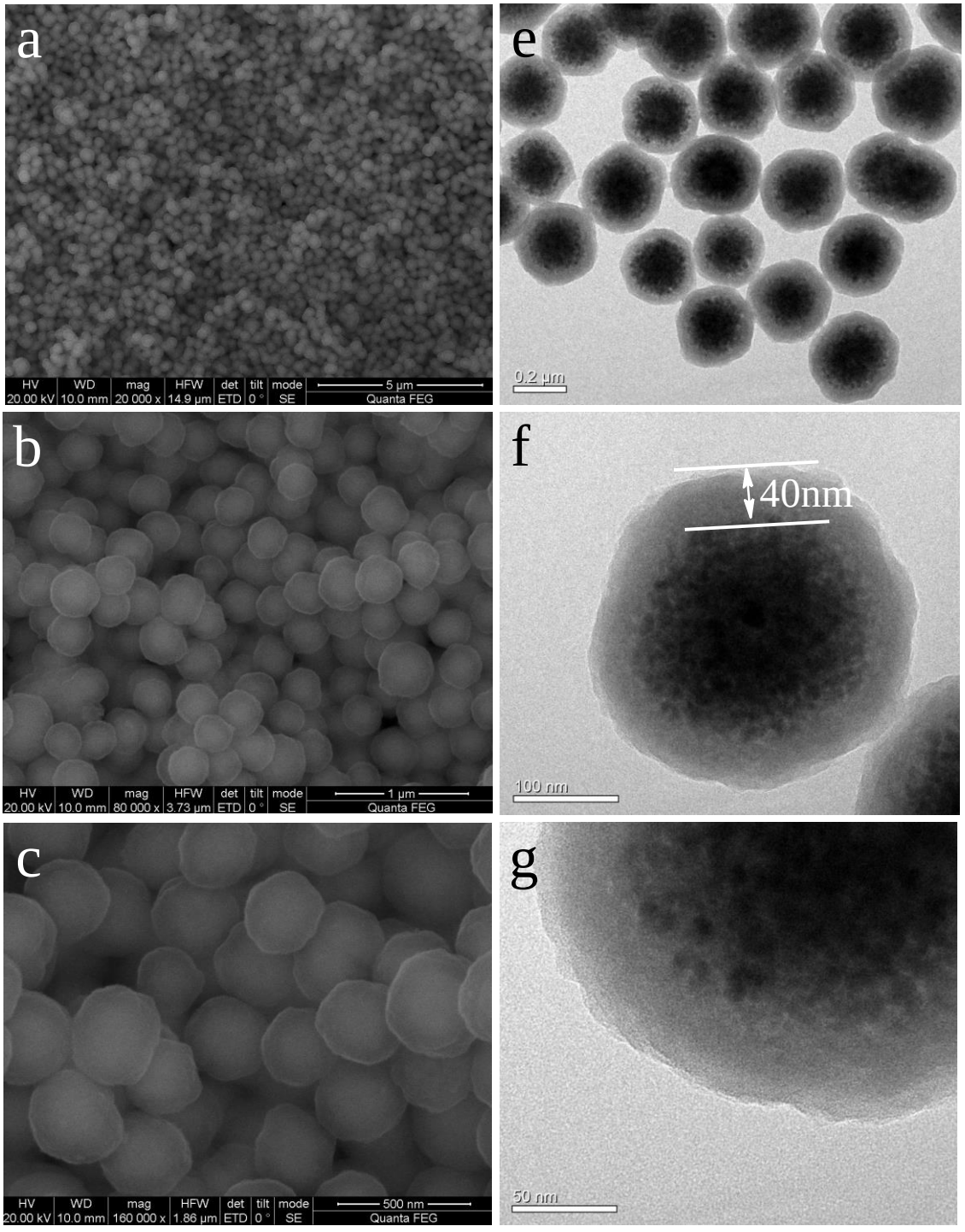

Figure 2. TEM (a, b, and c) and SEM (e, f, and g) images of Fe_3O_4@C nanostructures at different magnifications.

Fig. 3(a) shows the results of the EDS analysis carried out at the selected regions in Fig. 3(b). The EDS energy spectra were used to analyze the chemical composition of the material. According to the illustration in Fig. 3(a), it can be seen that the material consists of C, O, Si, and Fe elements. The relative percentage of "C", "O", "Si", and "Fe" elements were 45.15 %, 28.73 %, 0.74 %, and 25.38 %, respectively. This further confirmed the Fe_3O_4@C composition of the material.

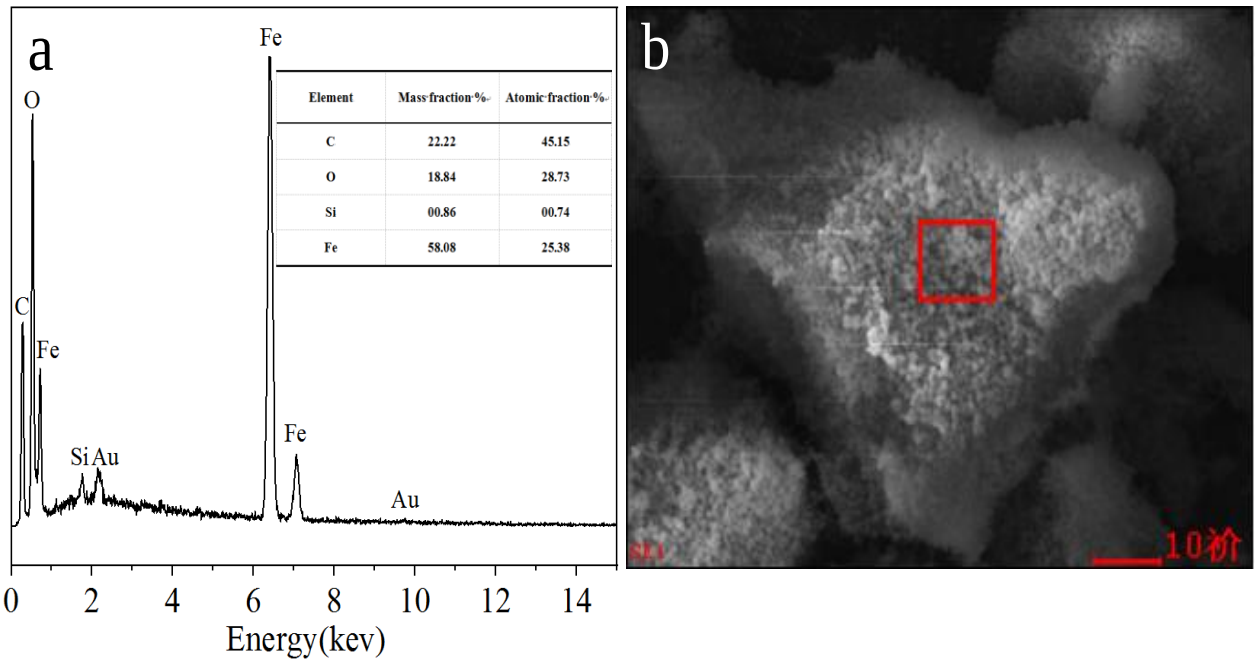

Element	Mass fraction/%	Atomic fraction/%
C	22.22	45.15
O	18.84	28.73
Si	00.86	00.74
Fe	58.08	25.38

Figure 3. EDS spectrum (a) and SEM image (b) of Fe_3O_4@C.

The cycling performance and coulombic efficiency of the Fe_3O_4@C nanospheres electrode at a constant current density of 100 mA g^{-1} are shown in Fig. 4a. At the end of the 100th cycle, the charge/discharge capacity remained at 539/544 mAh g^{-1} along with a coulombic efficiency of 99%. The above testing results of Fe_3O_4@C electrode are comparable to (even better than) those of Fe_3O_4-based electrodes reported in the literature [21, 22].Owing to the formation of the SEI layer and the decomposition of the electrolyte, the coulombic efficiency of Fe_3O_4@C nanosphere was only 57% in the first cycle, then quickly increased to 91% in the second cycle, and remained about 99% in the following cycles (Fig. 4a). It is interesting to note that the capacity first decreased but then slowly increased. The most possible cause of the capacity change was the degradation of the kinetically activated electrolyte[23]. Furthermore, the rate performance of the Fe_3O_4@C nanospheres is shown in Fig. 4b. With the current density increasing from 100 to 200, 500, and 1000 mA g^{-1}, the discharge capacities significantly declined from 801 to 681, 411, and 150 mAh g^{-1}, respectively. When the current density returned to 100 mA g^{-1} after 40 cycles, the discharge capacity returned to about 738 mAh g^{-1} without an obvious capacity loss. The results show that Fe_3O_4@C electrodes exhibit excellent

rate performance because the structure of uniform Fe_3O_4@C nanospheres remains fairly static and aids Li^+ transfer during the high-rate charge-discharge cycle[24].

CV measurement of the Fe_3O_4@C nanospheres electrode for the initial 10 cycles was carried out at a scan rate of 0.1 mV s^{-1} (Fig. 5a). There were two obvious peaks at about 0.61 and 2.01 V in the initial discharge process. The strong peak at 0.61 V reveals the irreversible reactions of the electrolyte to form the solid-electrolyte interphase layer. The small peak at 2.01 V can be ascribed to the lithiation reactions of Fe_3O_4 ($Fe_3O_4 + 8Li^+ + 8e- \rightarrow 3Fe^o + 4Li_2O$). In subsequent cycles, the reduction peaks of the reduction appeared at about 1.23 and 0.70 V during discharge. This is completely different from those of the 1st cycle, which can be attributed to the irreversible reactions with the formation of the SEI film[25]. Fe_3O_4@C nanospheres exhibit high coulombic efficiency, stability, and reversibility, which is due to the stable SEI film and the uniform carbon layer resulting in keeping the integrity of the Fe_3O_4 structure as well as preventing Fe_3O_4 nanoparticles from contacting the electrolyte[26]. For the charge process, the two oxidation peaks at about 1.61 and 1.94 V correspond to the electrochemical oxidation($Fe^o \rightarrow Fe^{2+}$ and $Fe^{2+} \rightarrow Fe^{3+}$). Moreover, the CV curves in the following cycles almost overlapped, indicating the high coulombic efficiency and excellent reversibility of the Fe_3O_4@C nanospheres electrode.

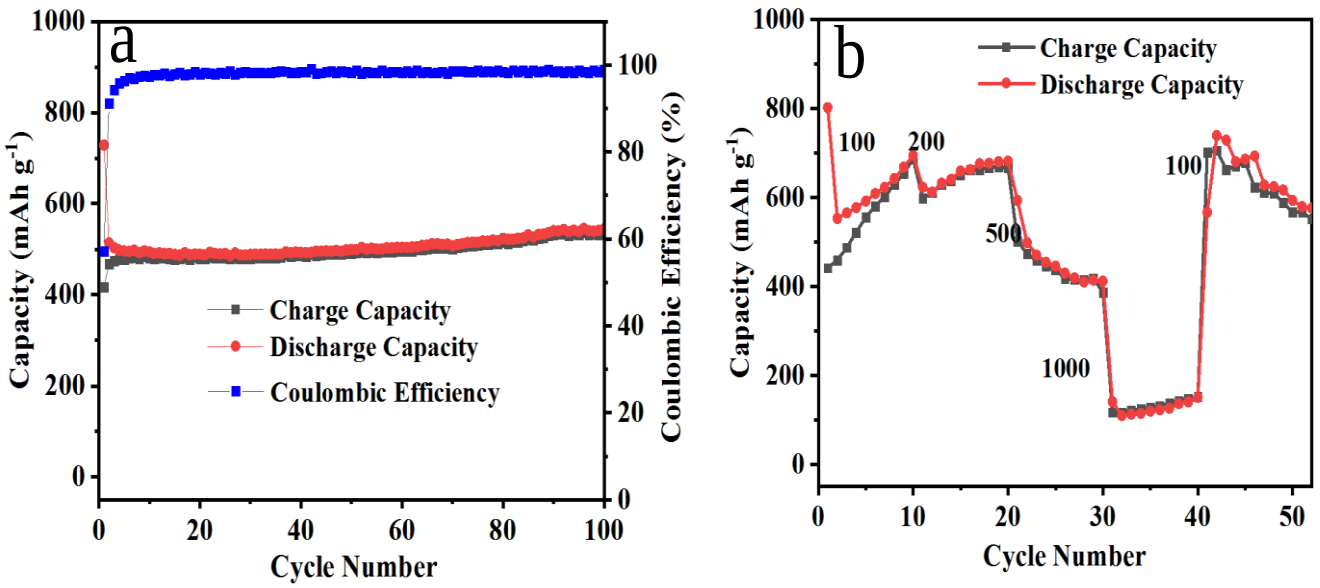

Figure 4. (a) Cycling performance and coulombic efficiency of Fe_3O_4@C at a current density of 100 mA g^{-1}; (b) rate performance at different current densities.

EIS measurements were carried out to further identify the electrochemical performance of Fe_3O_4@C nanospheres in the frequency range from 100 KHz to 0.01 Hz. From Fig. 5b, it can be seen that the diameter of the semicircle in the high frequency region is small, suggesting that the value of the charge transfer resistance and SEI film resistance are small. The resistance of the uniform Fe_3O_4@C nanosphere electrode was 17 Ω, which slowly increased to 28 Ω after 5 cycles and gradually increased to 35 Ω after 10 cycles, indicating that the carbon coating can enhance the structural stability

and help to improve the charge transfer ability[27]. The inclined line in the low frequency region shows that the diffusion of the lithium ion was fast. The EIS measurements were essentially in agreement with the cycling performance.

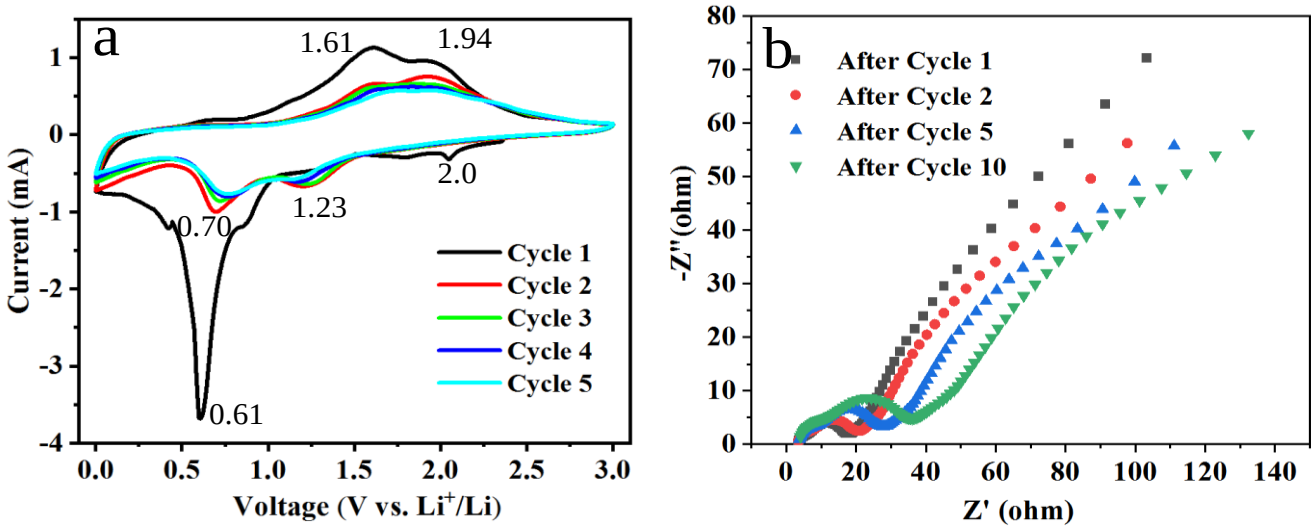

Figure 5. CV curves of Fe_3O_4@C at a scan rate of 0.1 mV s^{-1}; (b) Nyquist plots of Fe_3O_4@C in different cycles.

Table 1. Comparison of the electrochemical performance of iron oxide composites in the recently reported literature.

Materials	Reversible C_d (mAh g^{-1})/ Cycle number	Current density (mA g^{-1})	Ref.
bulk Fe_3O_4	90/100	0.1C	[28]
Fe_3O_4@C	480/100	0.1C	[28]
G- Fe_3O_4@C	860/100	0.1C	[28]
Fe_3O_4/C	610/50	100	[29]
Fe_3O_4/C	430/100	100	[30]
Fe_3O_4/C	471/100	100	[31]
Fe_3O_4/C-600 nanosheets	647/100	100	[32]
Carbon-Coated Fe_3O_4@Fe_2SiO_4	522.2/100	100	[33]
OH-Fe_3O_4@NC	1316/50	100	[34]
Fe_3O_4@C	891.2/100	0.2C	[25]
Fe_3O_4@C	640.5/1000	2C	[25]
Fe_3O_4@C	539/100	100	this work

The electrochemical characteristic of similar materials previously reported are listed in Table 1. It can be seen that the Fe_3O_4@C nanospheres in this work exhibit the optimal electrochemical

performance with good cycling stability and high reversible specific capacity which were synthesized by a one-step solvothermal method. As can be seen form the table, fabricated Fe_3O_4/C nanocomposites have a better rate capability with excellent cycle stability than those of pure Fe_3O_4 nanocrystals. As a result, uniform Fe_3O_4@C nanospheres in the present work efficiently improved the cycling stability and Coulombic efficiency, which verifies that these nanocomposites are promising for LIBs.

4. CONCLUSIONS

In summary, we developed a facile one-step solvothermal method to synthesize highly uniform Fe_3O_4@C nanospheres. The microstructure, morphology, and chemical composition of the obtained Fe_3O_4@C nanospheres were characterized by XRD, SEM, EDS, and TEM. The electrochemical measurements prove that the uniform Fe_3O_4@C nanospheres electrode exhibits good reversible capacity and excellent cycling stability (539/544 mAh g^{-1} at a current density of 100 mA g^{-1} after 100 cycles). In addition, the capacity retention was 129% of the initial charge capacity. The improved reversible capacity and Li^+ diffusion performance are due to the small size of Fe_3O_4@C nanospheres and the uniform carbon layer. This work is helpful to develop high-performance iron-base nanocomposites LIB anode material.

ACKNOWLEDGMENTS
The authors acknowledge financial supports from the Program of Zaozhuang Science and Technology Development Plan (2016GX34), the PhD Research Startup Foundation of Zaozhuang University (1020711), and the Scientific Research Foundation of Zaozhuang University (102061802). Thanks to Yi Hu, China University of Mining and Technology, for testing advice. Thanks to Dr. Edward C. Mignot, Shandong Uniwersity, for linguistic advice.

References

1. Y. Pana, W. J. Zeng, L. Li, Y. Z. Zhang, Y. N. Dong, K. Ye, K. Cheng, D. X. Cao, G. L. Wang, B. L. Lucht, *J. Electroanal. Chem*., 810 (2018) 248.
2. S. Huang, J. W. Zhang, L. Yang, C. H. Gong, J. H. Guo, P. Y. Zhang, Q. W. Li, K. F. Huo, L. Q. Mai, J. J. Yang, J. W. Zhang, *J. Alloys Compd*., 800 (2019)16.
3. W. Deng, S. Q. Ci, H. Li, Z. H. Wen, *Chem. Eng. J*., 330 (2017) 995.
4. Y. R. Li, R. Y. Wang, J. W. Zhang, J. P. Chen, C. Q. Du, T. H. Sun, J. Liu, C. H. Gong, J. H. Guo, L. G. Yu, J. W. Zhang, *Ceram. Int.*, 45 (2019) 16195.
5. Y. L. Liu, Y. P. Wang, A. Q. Pan, *Int. J. Electrochem. Sci*., 12 (2017) 2506.
6. M. Liu, H. Y. Jin, E. Uchaker, Z. Q. Xie, Y. Wang, G. Z. Cao, S. E. Hou and J. Y. Li, *Nanotechnol.*, 28 (2017) 155603.
7. C. Guo, L. L. Wang, Y. C. Zhu, D. F. Wang, Q. Q. Yang and Y. T. Qian, *Nanoscale*, 7 (2015) 10123.
8. L. Y. Sun, L. Yang, J. Li, R. L. Narayan, X. H. Ning, *Electrochim. Acta*, 288 (2018) 71.
9. H. Liu, S. H. Luo, D. B. Hu, X. Liu, Q. Wang, Z. Y. Wang, Y. L. Wang, L. J. Chang, Y. G. Liu, T. F. Yi, Y. H. Zhang, A. M. Hao, *Appl. Surf. Sci*., 495 (2019) 143590.
10. Y. Zeng, J. Z. Luo, Y. Z. Wang, L. Qiao, B. Zou, W. T. Zheng, *Nanoscale*, 9 (2017) 17576.

11. D. S. Li, Y. Zhang, K. Rui, H. J. Lin, Y. Yan, X. S. Wang, C. Zhang, X. Huang, J. X. Zhu and W. Huang, *Nanotechnol*., 30 (2019) 094002
12. W. H. Ren, D. N. Liu, C. L. Sun, X. H. Yao, J. Tan, C. M. Wang, K. N. Zhao, X. P. Wang, Q. Li, L. Q. Mai, *Small*, 14 (2018) 1800659.
13. Y. Suo, Q. Q. Zhao, J. K. Meng, J. Li, X. C. Zheng, X. X. Guan, Y. S. Liu, J. M. Zhang, *Mater. Lett.*, 174 (2016) 36.
14. C. L. Ma, J. Shi, Y. Zhao, N. J. Song, Y. X. Wang, *Chem. Eng. J*., 326 (2017) 507.
15. Y. Zhang, Y. K. Tang, S. S. Gao, D. Z. Jia, J. H. Ma, and L. Liu, *ACS Appl. Mater. Interfaces*, 9(2017) 1453.
16. H. Luo, K. Huang, B. Sun, J. X. Zhong, *Electrochim. Acta*, 149 (2014) 11.
17. G. X. Gao, S. Y. Lu, B. T. Dong, Z. C. Zhang, Y. S. Zheng, S. J. Ding, *J. Mater. Chem.* A, 3 (2015) 4716.
18. Y. Z. Wan, Z. W. Yang, G. Y. Xiong, R. S. Guo, Z. Liu, H. L. Luo, *J. Power Sources*, 294 (2015) 414.
19. C. Wu, Q. C. Zhuang, L. L. Tian, Y. L. Cui, X. X. Zhang, *Mater. Lett.*, 107 (2013) 27.
20. Y. L. Wang, J. Yu, R. Li, Q. Zhen, *Prog. Chem.*, 24 (2012) 2132.
21. D. Wang, L. Jiang, X. Wei, C. Song, *Mater. Lett.*, 138 (2015) 164.
22. D.H. Lee, S.D. Seo, G.H. Lee, H.S. Hong, D.W. Kim, J. Alloy. Compd. 606 (2014) 204.
23. F. Wang, C. Q. Wang, H. Chen, W. L. Zhang, R. J. Jiang, Z. H. Yan, Z. Y. Huang, H. H. Zhou, Y. F. Kuang, *Nanotechnol.*, 30 (2019) 335701.
24. Q. H. Wu, R. F. Zhao, W. J. Liu, X. E. Zhang, X. Shen, W. L. Li, G. W. Diao, M. Chen, *J. Solid State Chem.*, 344 (2017) 74.
25. Y. Yu, Y. C. He, N. Xu, X. L. Geng, L. Y. Wang, H. T. Sun, L. H. Zhu, Z. H. Jing, *J. Solid State Chem.*, 271 (2019) 121.
26. J. Du, Y. Ding, L. G. Guo, L. Wang, Z. B. Fu, C. Q. Qin, F. Wang, X. Y. Tao, *Appl. Surf. Sci.*, 425 (2017) 164.
27. X. L. Shi, Q. Q. Yao, H. F. Wu, Y. Zhao, L. H. Guan, *Nanotechnol.*, 30 (2019) 465402.
28. L. Zhao, M. M. Gao, W. B. Yue, Y. Jiang, Y. Wang, Y. Ren, F. Q. Hu, *ACS Appl. Mater. Interfaces*, 7 (2015) 9709.
29. X. Y. Chen, B. H. Liu, Z. P. Li, *Solid State Ionics*, 261(2014) 45.
30. P. Wang, M. X. Gao, H. G. Pan, J. L. Zhang, C. Liang, J. H. Wang, P. Zhou, Y. F. Liu, *J. Power Sources*, 239 (2013) 466.
31. M. J. Hu, Y. Z. Jiang, M. Yan, *J. Alloys Compd*., 582 (2014) 563.
32. Q. Xin, L. G. Gai, Y. Wang, W. Y. Ma, H. H. Jiang, Y. Tian, *J. Alloys Compd*., 691 (2017) 592.
33. X. X. Yang, J. Qiu, *Mater. Res. Express*, 5 (2018) 095504.
34. Y. Wang, L. Chen, H. T. Liu, Z. M. Xiong, L. Zhao, S. H. Liu, C. M. Huang, Y. M. Zhao, *Chem. Eng. J*., 356 (2019) 746.